

PAPER • OPEN ACCESS

A Millimetre-wave Probe for Fast Screening and Evaluation of Corrosion in Planar Conductors: Numerical Simulations

To cite this article: Wenjia Li *et al* 2019 *IOP Conf. Ser.: Mater. Sci. Eng.* **554** 012003

View the [article online](#) for updates and enhancements.

A Millimetre-wave Probe for Fast Screening and Evaluation of Corrosion in Planar Conductors: Numerical Simulations

Wenjia Li¹, Yong Li^{1,*}, Jianguo Tan¹, Ilham Mukriz Zainal Abidin²,
Jinhua Hu¹, Zhenmao Chen¹, Yongzhuo Wu³

¹ State Key Laboratory for Strength and Vibration of Mechanical Structures, Shaanxi Engineering Research Centre of NDT and Structural Integrity Evaluation, School of Aerospace Engineering, Xi'an Jiaotong University, Xi'an, Shaanxi, China

² Leading Edge NDT Technology (LENDT) Group, Malaysian Nuclear Agency, 43000 Bangi, Kajang, Selangor, Malaysia

³ Jiangsu Eqotek Testing Services Co. Ltd, Kunshan, Jiangsu, China

Corresponding author, email: yong.li@mail.xjtu.edu.cn

Abstract. Planar conductors are commonly used in critical mechanical structures. Due to high-temperature and high-pressure environment, corrosion may occur in in-service planar conductors, and seriously threatens structural integrity and safety. Hence, it is indispensable to detect and evaluate corrosion using Non-destructive Testing (NDT) techniques before structural failure. As a technique complementary to other Electromagnetic NDT methods, Microwave NDT is found to be advantageous in terms of high efficiency and accuracy in inspection of conductors subject to surface flaws. In this paper, a millimetre-wave probe for efficient detection and evaluation of corrosion in planar conductors is proposed and intensively investigated via simulation. A 3D Finite Element (FE) model of the proposed probe is established based on electromagnetic wave theory. The characteristics of the microwave propagation along with the mechanism regarding corrosion detection are intensively analysed. The probe structure and parameters are subsequently optimised in an effort to enhance the detectability, sensitivity and accuracy in corrosion evaluation. Besides, signal processing techniques involving extraction of features from the S-parameter in the function of frequency are investigated.

1. Introduction

Planar conductors are commonly used in critical mechanical structures. Due to high-temperature and high-pressure environment, corrosion may occur in in-service planar conductors, and seriously threatens structural integrity and safety. Hence, periodic non-destructive testing for planar conductors in large complex structures plays a key role to guarantee the safety and reliability of the structures. Conventional non-destructive testing methods mainly include Radiographic Testing (RT) [1], Eddy Current Testing (ECT) [1] and Ultrasonic Testing (UT) [2]. RT may be pernicious to inspectors, and thus protective measure must be taken. ECT is scarcely efficient and susceptible to interference from the material itself and other factors. UT requires coupling agent deployed over the surface of the specimen, and is merely applicable for the detection of subsurface defects. As a complementary technique to other Electromagnetic Non-destructive Testing (NDT) methods, Microwave NDT has the advantage over conventional methods in efficiency and sensitivity [3].



A typical Microwave NDT system is normally comprised of a microwave generator, coaxial cables and probes. The generator is used for generating the microwave, the coaxial cables are the connector between the generator and the probes, and the probes are the key components for transmitting and receiving the microwave [4]. The probes used for microwave NDT generally include horn antennas [5], waveguides [6] and coaxial line sensors [7,8,9]. Since the propagation direction of the microwave transmitted by the probe is perpendicular to the specimen surface, the probe should be scanned over the specimen surface with small steps to achieve high-spatial-resolution inspection [10]. This makes it inefficient to use these probes for Microwave NDT. Therefore, it is highly desirable to develop a new type of Microwave NDT probe with high detection efficiency and sensitivity.

This paper proposed a new probe working in K-band (i.e. a millimetre-wave probe) for detection and evaluation of corrosion in planar conductors. The probe consists of a rectangular metal box in which part of the bottom surface is in absence, and an excitation port (Coaxial Port #1) and a detection port (Coaxial Port #2) both embedded on the upper surface of the metal box. The probe ports are connected with the vector network analyser for microwave excitation and acquisition. Figure 1 illustrates the schematic diagram of the Microwave NDT system together with the cross-sectional view (along y -axis) of the proposed probe. The detection principle underlying the proposed probe is that the excited microwave horizontally propagates in the waveguide structure which is composed of the probe metal box and the upper surface of the planar conductor under inspection. The corrosion occurring in the conductor surface perturbs the transmission of the microwave from the excitation port to detection port. This results in the variations in: (1) the transmitted microwave received by the detection port; and (2) the reflected wave captured by the excitation port. Compared with the scenario for flawless conductors, the resulting signals, which are the S-parameters (i.e. S_{11} and S_{21} [11]) in the function of excitation frequency, consequently vary with the presence of corrosion, giving implication regarding corrosion parameters.

In the rest of this paper, the intrinsic mechanism regarding the detection and evaluation of corrosion by using the proposed probe is analysed via Finite Element (FE) simulations. Based on this, the probe is further optimised particularly regarding the matching port, metal ring of the coaxial port and detection mode. The correlations of signals of S_{11} and S_{21} and their features with the corrosion parameters are subsequently investigated.

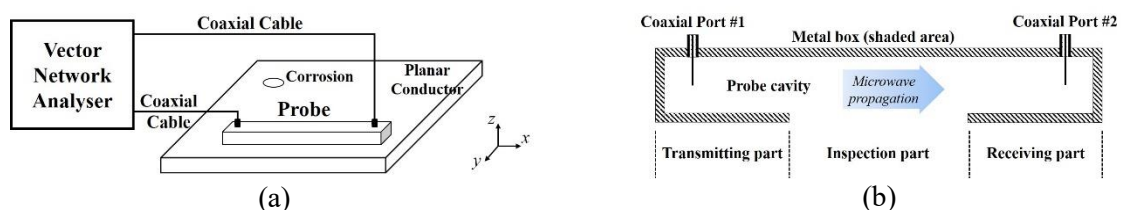


Figure 1. (a) Schematic diagram of the system along with the proposed millimetre-wave probe. (b) Cross-sectional illustration of the proposed probe.

2. Numerical simulations

In a bid to investigate the characteristics of millimetre-wave propagating in the probe and optimisation of probe parameters, a 3D Finite Element (FE) model has been built up based on finite element modelling. A series of FE simulations are intentionally conducted subsequently. It should be noted that the model is solved with approximately 835,164 tetrahedral elements.

2.1. Model setup.

2.1.1. The wave equation and material settings.

The model with the proposed probe deployed over a planar conductor is illustrated in Figure 2(a). In the simulation, the field quantity i.e. electric field intensity \mathbf{E} is obtained by numerically solving the wave equation of microwave propagation in the air, dielectric material and conductor. The wave equation is written as [12]:

$$\nabla \times \mu_r^{-1} (\nabla \times \mathbf{E}) - k_0^2 \left(\epsilon_r - \frac{j\sigma}{\omega\epsilon_0} \right) \mathbf{E} = 0 \quad (1)$$

where, μ_0 and ϵ_0 represent the permeability and dielectric constant of vacuum, respectively. μ_r , ϵ_r and σ indicate the relative permeability, relative dielectric constant and electrical conductivity of a material in the model. ω denotes the angular frequency. k_0 is the wave number.

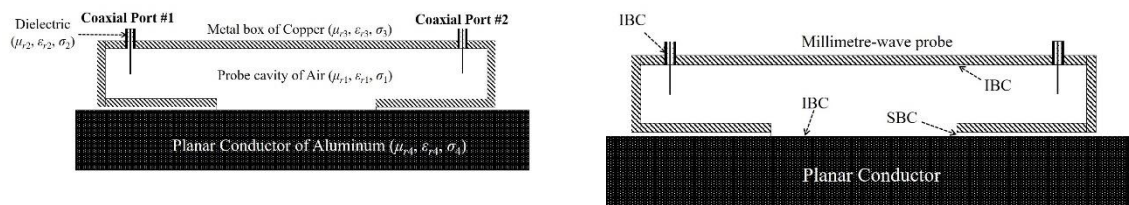


Figure 2. (a) The material for each region by cross-sectional illustration. (b) Setup of the boundary conditions.

In Figure 2(a), the material in the probe cavity is air whilst the material of the coaxial port region is dielectric. The material of the metal box of the probe is copper whilst the planar conductor under inspection is an aluminium slab. The material properties of the air, dielectric material, copper and aluminium involved in simulations are listed in Table 1.

Table 1. Properties of the materials involved in simulations.

Material	Property	Name	Value
Air	Relative permeability	μ_{r1}	1
	Dielectric constant	ϵ_{r1}	1
	Electrical conductivity	σ_1	0 S/m
Dielectric Material	Relative permeability	μ_{r2}	1
	Dielectric constant	ϵ_{r2}	2
	Electrical conductivity	σ_2	0 S/m
Copper	Relative permeability	μ_{r3}	1
	Dielectric constant	ϵ_{r3}	1
	Electrical conductivity	σ_3	59.98 MS/m
Aluminium 6063-T83	Relative permeability	μ_{r4}	1
	Dielectric constant	ϵ_{r4}	1
	Electrical conductivity	σ_4	30.30 MS/m

2.1.2. Boundary conditions.

The behaviour of the microwave at the interface between 2 different materials is important for analysis of electromagnetic phenomena, and constituted by boundary conditions. The setup of the boundary conditions regarding the FE model is illustrated in Figure 2(b). In the model, the Impedance Boundary Condition (IBC) is firstly applied to the interfaces between the metal and dielectric material in light of the fact that there is impedance loss at the interface.

It is noted that the use of IBC is based on the assumption that the skin depth of the electromagnetic field in the conductor under microwave illumination is much less than the conductor thickness. Therefore, IBC can only be applied to the surface of the conductor with the thickness considerably larger than the skin depth. The IBC is written as [12]:

$$\sqrt{\frac{\mu_0 \mu_r}{\epsilon_c}} \mathbf{n} \times \mathbf{H} + \mathbf{E} - (\mathbf{n} \cdot \mathbf{E}) \mathbf{n} = (\mathbf{n} \cdot \mathbf{E}_s) \mathbf{n} - \mathbf{E}_s \quad (2)$$

where, the source electric field \mathbf{E}_s can be used to specify a source surface current on the boundary. In addition to the boundary conditions between the metal and the media, there is a certain gap between the probe and the planar conductor (namely probe lift-off), which causes the leakage of microwave. Since only the distribution of electromagnetic wave in the waveguide structure composed of the probe metal box and planar conductor is concerned, the Scattering Boundary Condition (SBC) directly absorbs the microwaves leaking from the outward radiation is applied, which is expressed as [12]:

$$\mathbf{E} = \mathbf{E}_{sc} e^{-ik(\mathbf{n} \cdot \mathbf{r})} + \mathbf{E}_0 e^{-ik(\mathbf{k} \cdot \mathbf{r})} \quad (3)$$

where, the field \mathbf{E}_0 is the incident plane wave that travels in the direction \mathbf{k} .

With the consideration of the wave equation for microwave propagation and the boundary conditions, the model is thus completely established, and subsequently solved via FEM.

2.2. Probe optimisation.

2.2.1. Optimisation regarding the port matching.

Simulations have been firstly conducted in a bid to optimise the structure of the transmitting/receiving part of the probe for efficient transmission of microwave from the coaxial port to the inspection part. Note that as indicated in Figure 1(b), the transmitting/receiving part of the probe consists of a coaxial port and cuboid similar to waveguide structure. Three types of the structures including the rectangular port, open port and quarter-wavelength waveguide are investigated in simulations, and portrayed in Figure 3. For each structure, S_{11} depicting the energy of the microwave reflected to the excitation port is simulated and analysed. The simulation results are presented in Figure 4.

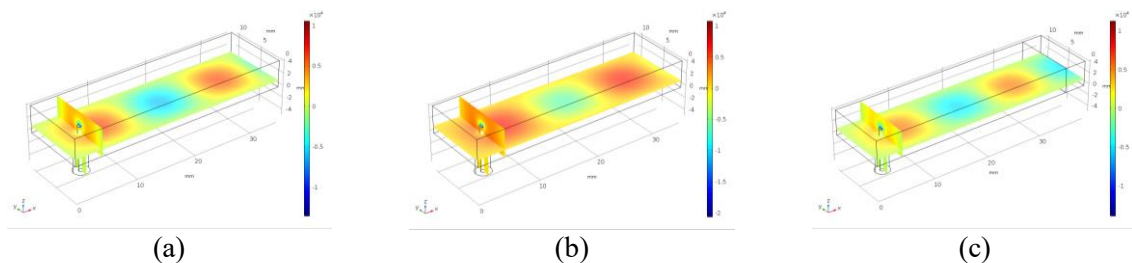


Figure 3. Structures of the transmitting part of the proposed probe: (a) The rectangular port; (b) Open Circuit port; and (c) Quarter-wavelength waveguide.

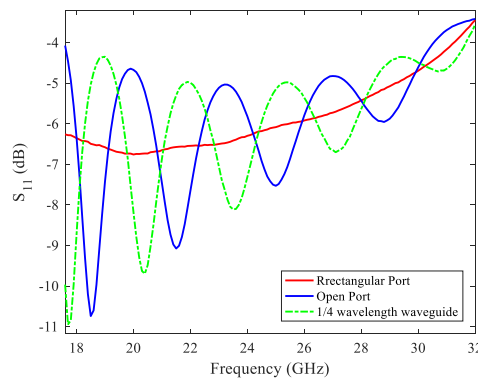


Figure 4. S_{11} vs. frequency for three types of the structures of the transmitting part: the rectangular port, open port and quarter-wavelength waveguide

It can be found from Figure 4 that for the entire frequency range, compared with the significant fluctuation in S_{11} for the open-circuit matching structure and the quarter-wavelength waveguide, the value of S_{11} for the rectangular port is relatively stable. This reveals that the rectangular port is stable over the frequency band of the proposed probe, and gives relatively low S_{11} value. This can be taken as the preferred matching option. The simulation result indicating the field distribution along with the energy flow of the microwave propagating through the rectangular-port-based transmitting part of the probe is presented in Figure 5. It can be seen that the electric field intensity distribution in the transmitting part of the probe is uniform, and a large amount of microwave energy in the transmitting part of the probe is transmitted to the detection area. The designed metal ring plays an indispensable role in the efficient excitation and transmission of the microwave.

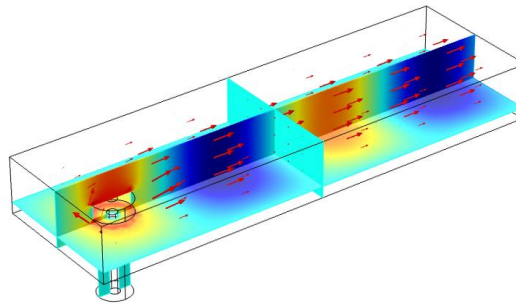


Figure 5. Distributions of the electric field and energy flow of the microwave propagating in the probe cavity.

2.2.2. Optimisation of the metal ring.

In an effort to improve and probe excitation performance and enhance the transmission of microwave, a metal ring is usually introduced to the coaxial port of a microwave NDT probe. As a result, the metal ring added to each coaxial port of the proposed probe is taken into account in the model. The size of the metal ring in terms of l_{mr} for the height of the metal ring and r_{mr} for the ring radius are thus optimised by S_{11} acquired from simulations. The sizes of the metal ring and the corresponding S_{11} against different excitation frequencies are listed in Table 2.

Table 2. The size of metal ring and S_{11} vs. excitation frequency

Excitation frequency (GHz)	l_{mr} (mm)	r_{mr} (mm)	S_{11} (dB)
20	1.30	0.95	-45
21	0.95	2.15	-33
22	0.70	1.60	-49.6
23	0.85	1.10	-39
24	0.95	1.55	-40
25	0.60	1.60	-40

From Table 2, it can be seen that S_{11} at the excitation frequency of 22GHz is minimum when the metal ring size is 0.7mm×1.6mm ($l_{mr} \times r_{mr}$). This indicates that such metal ring size corresponding to -49.6dB could be preferable. Whereas, in consideration of the fabrication and centre frequency of the operation band of the probe (approx. 23GHz), the preferred size of the metal ring is 0.85mm×1.10mm.

2.3. Characteristics of the microwave propagation in the probe.

After the optimisation of the critical parts of the probe, the microwave propagation within the probe cavity is simulated. The distribution and electric field and power flow of the microwave are investigated together with the simulated S_{11} and S_{21} which are acquired at Coaxial Port #1 and Coaxial Port #2, respectively. The simulation results are presented in Figure 6.

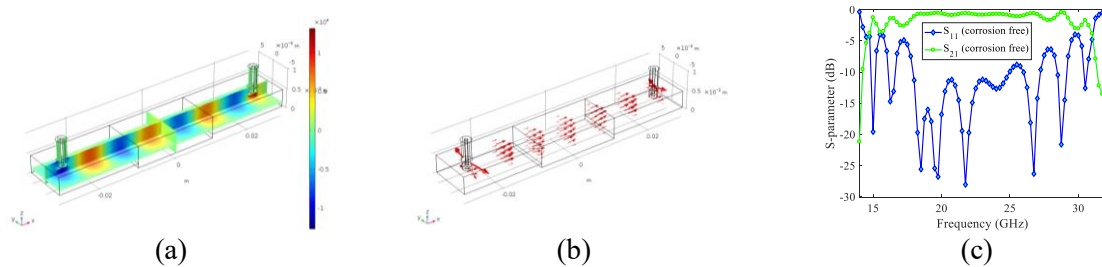


Figure 6. Simulation results: (a) z component of electric field intensity in the probe; (b) power flow inside the probe; and (c) S-parameters for the probe placed on the flawless conductor.

From Figure 6(a)-(b), it can be seen that a large majority of the microwave energy is transmitted from Coaxial Port #1 to Coaxial Port #2. This facilitates the detection and evaluation of corrosion in the planar conductor which is illuminated by incident wave from the inspection part of the proposed probe. It is also noticeable from Figure 6(c) that when the conductor is free of corrosion, the amplitude of S_{11} is considerably higher than that of S_{21} . This implies the high efficiency of the microwave propagating through the probe. Since S_{11} and S_{21} could vary in the presence of corrosion, they are subsequently utilised for corrosion evaluation.

3. Detection and evaluation of corrosion using the proposed probe

After the design and optimisation of the probe, FEM simulations are conducted for investigation of corrosion evaluation based on signals of S_{11} and S_{21} . Corrosion in the cylindrical shape with variable depths and radii are taken into account in simulations.

3.1. Corrosion in different depths

Corrosion in different depths is firstly considered in simulations. The depth of the corrosion h_c varies from 1mm to 5mm whilst its radius is fixed at 2mm. The simulated signals of S_{11} and S_{21} against different corrosion depths are shown in Figure 7. It can be found that the detection probe is sensitive to the depth of corrosion. For the corrosion with variable depth, the S-parameter signals changes significantly compared with the corrosion-free case. This indicates the capability of the proposed probe in detection and evaluation of corrosion in planar conductors. It is also noticeable from Figure 7 that the variation in the signal of S_{11} is more significant than that in the S_{21} signal, which implies that the S_{11} -based evaluation of corrosion depth could have more sensitivity than that based on S_{21} . This opens up the sensitivity analysis regarding S-parameters in detection and evaluation of corrosion.

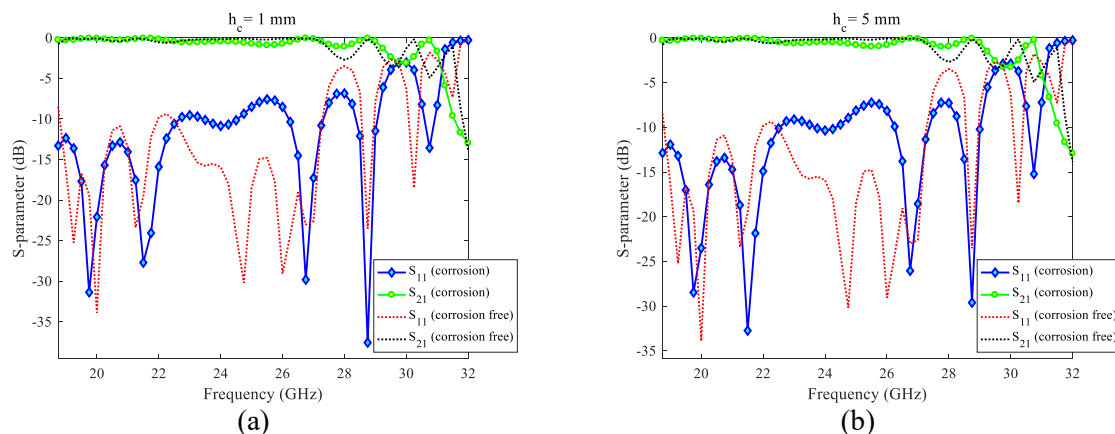


Figure 7. Simulated signals of S_{11} and S_{21} for corrosion with the depth of: (a) 1mm; and (b) 5mm

In order to estimate the depth of corrosion, it is indispensable to extract signal features from the acquired signals. A new feature based on the excitation frequency and S-parameters is proposed, and calculated via:

$$F_1 = \sum_{f_o=f_{start}}^{f_o=f_{end}} (f_o \cdot S_{21}); F_2 = \sum_{f_o=f_{start}}^{f_o=f_{end}} (f_o \cdot S_{11}) \quad (4)$$

where, f_{start} and f_{end} are the starting and stopping frequencies of the frequency band, respectively. f_o denotes the operating frequency whilst S_n ($n=21, 11$) is the corresponding S parameter at the operating frequency. The correlations of the computed F_1 and F_2 with the corrosion depth are shown in Figure 8(a). It is noteworthy that when computing F_1 and F_2 , $f_{start}=18.75\text{GHz}$ and $f_{end}=32\text{GHz}$. It can be seen from Figure 8(a) that both F_1 and F_2 have monotonic relations with the corrosion depth. When the corrosion depth increases, F_1 decreases whilst F_2 rises. The reasoning behind is that as the depth of the defect increases, the standing wave remaining in the corrosion region increases. This results in the increase and drop in magnitude/power of the transmitted and reflected waves, respectively. In consequence, S_{21} and the resulting F_1 decreases whilst S_{11} and the resulting F_2 increases. The sensitivity analysis regarding F_1 and F_2 is conducted via subtraction of F_1 and F_2 in the presence of corrosion into those for corrosion-free scenario, giving the differential feature. The comparison is shown in Figure 8(b). As can be seen in Figure 8(b) that the difference in F_1 is less than that in F_2 , which indicates that F_2 is more sensitive to corrosion with variable depth than F_1 . This could be because the signal strength of S_{11} is higher than that of S_{21} .

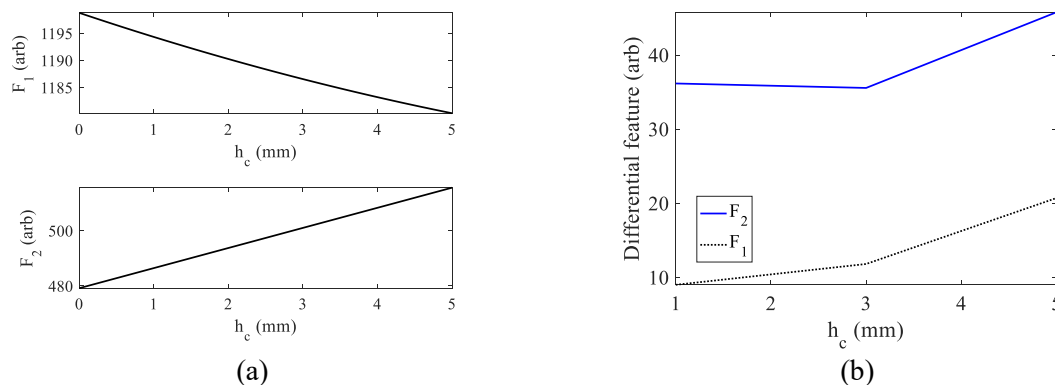


Figure 8. Analysis and comparison regarding: (a) correlations of the computed F_1 and F_2 with the corrosion depth; and (b) Differences of F_1 and F_2 in the presence of corrosion.

3.2. Corrosion in various volumes

Further investigation is focused on evaluation of corrosion with different volumes v_c . For such case, the corrosion radius varies from 1mm to 5mm whilst its depth is comparable to the radius. The simulated signals of S_{11} and S_{21} against different corrosion volumes (from 3.14mm^3 to 392.67mm^3) are shown in Figure 9. It can be seen from Figure 9 that the probe can hardly detect corrosion whose volume is 3.14mm^3 . Whereas, as the corrosion volume increases, significant variation in the S-parameter signal can be found. As a result, the corrosion volume could be quantitatively evaluated based on F_1 and F_2 .

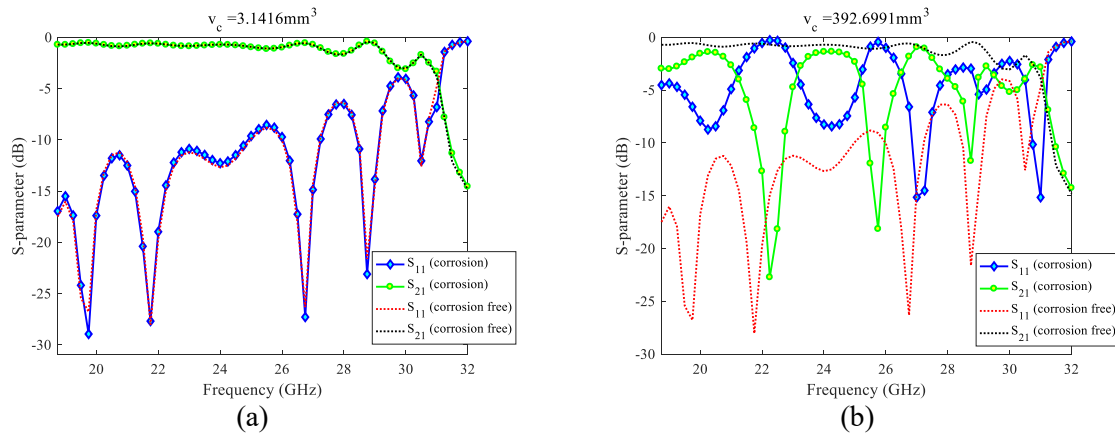


Figure 9. Simulated signals of S_{11} and S_{21} for corrosion with the volume of: (a) 3.14mm^3 ; and (b) 392.5mm^3

The correlation of the computed F_1 and F_2 with the corrosion volume are presented in Figure 10(a). It can be found from Figure 10(a) that both F_1 and F_2 have monotonic relations with the corrosion volume. When the corrosion volume rises, F_1 decreases whilst F_2 rises, which can be explained by the fact presented in Section 3.1. Figure 10(b) presents the sensitivity analysis and comparison of F_1 with F_2 for evaluation of corrosion volume. It can be found in Figure 10(b) that similar to the finding presented in Section 3.1, F_2 has higher sensitivity to corrosion with different volumes than F_1 . Therefore, F_2 could be preferred for high-accuracy evaluation and imaging of corrosion in planar conductors.

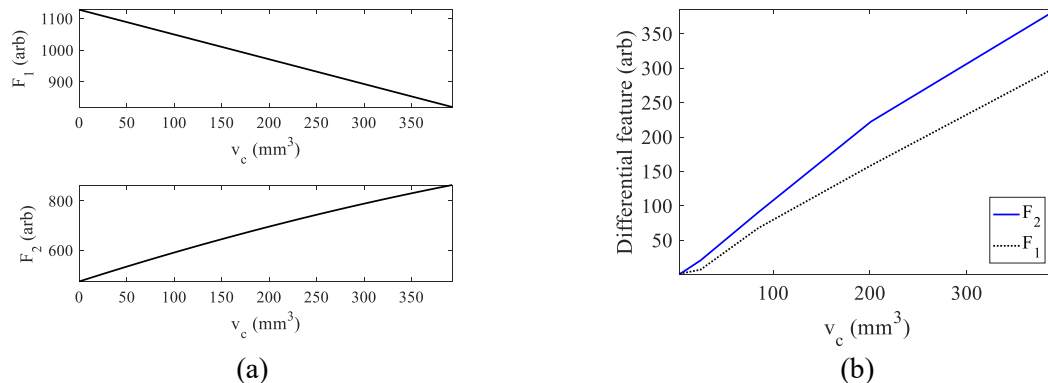


Figure 10. Analysis and comparison regarding: (a) correlations of the computed F_1 and F_2 with the corrosion volume; and (b) Differences of F_1 and F_2 in the presence of corrosion.

4. Conclusion

In this paper, a new K -band probe has been proposed for fast screening and evaluation of corrosion in planar conductors. A 3D FE model of the proposed probe is established. Based on the model, a series of simulations are carried out for analysis of the mechanism regarding corrosion detection and characteristics of the microwave propagation within the probe cavity. The structures of 2 critical parts of the probe, i.e. the matching port and metal ring are subsequently optimised. Following this, the correlation of the testing signal of the S-parameter with corrosion in different depths and radii is intensively investigated via simulations. A new feature based on the excitation frequency and S-parameter has been proposed for corrosion evaluation. It has been found from the simulation results that the features extracted from the testing signals have monotonic relations with the depth and radius of corrosion. This would benefit the comprehensive evaluation and imaging of corrosion in planar conductors.

Acknowledgments

The authors would like to thank the Natural Science Foundation of China (Grant No. 51777149, 51477127), National Key R&D Program of China (Grant No. 2017YFF0209703), and Fundamental Research Funds for the Central Universities of China (Grant No. XJJ2018027).

References

- [1] Deng Y and Liu X 2011 Electromagnetic imaging methods for nondestructive evaluation applications *Sensors* **11** 11774-808
- [2] Castellano A, Foti P, Fraddosio A, Galietti U, Marzano S and Piccioni M 2015 Characterization of Material Damage by Ultrasonic Immersion Test *Procedia Engineering* **109** 395-402
- [3] Zhang H, Gao B, Tian G, Woo W and Bai L 2013 Metal defects sizing and detection under thick coating using microwave NDT *NDT&E International* **60** 52-61
- [4] Liu L 2010 Remote Detection and Quantitative Evaluation of Wall Thinning Volumes in a Metal Pipe *EJAM* **2** 101-109
- [5] Ziehm C, Hantscher S, Hinken J, Ziep C and Richter M 2016 Near field focusing for nondestructive microwave testing at 24 GHz – Theory and experimental verification *Case Studies in Nondestructive Testing and Evaluation* **6** 70-78
- [6] Yang Y, He C and Wu B 2013 Non-destructive microwave evaluation of plasma sprayed TBCs porosity *NDT&E International* **59** 34-39
- [7] Liu L, Ju Y, Chen M and Fang D 2011 Application of Microwaves for Nondestructive and High-Efficiency Detection of Wall Thinning Locations in a Long-Distance Metal Pipe *Materials Transactions* **52** 2091-97
- [8] Liu L, Ju Y and Chen M 2013 Optimizing the frequency range of microwaves for high-resolution evaluation of wall thinning locations in a long-distance metal pipe *NDT&E International* **57** 52-57
- [9] Liu L and Ju Y 2011 A high-efficiency nondestructive method for remote detection and quantitative evaluation of pipe wall thinning using microwaves *NDT&E International* **44** 106-110
- [10] Yang S, Kim K and Kang J 2013 Detection of surface crack in film-coated metals using an open-ended coaxial line sensor and dual microwave frequencies *NDT&E International* **54** 91-95
- [11] Sakai Y, Yusa N and Hashizume H 2012 Nondestructive evaluation of wall thinning inside a pipe using the reflection of microwaves with the aid of signal processing *NONDESTRUCT TEST EVAL* **27** 171-184
- [12] Ida N 1992 *Microwave NDT* (SPRING SCIENCE+BUSINESS MEDIA, B.V.)